J. Fluid Mech. (2021), *vol*. 913, R1, doi:10.1017/jfm.2021.71

Intermediate scaling and logarithmic invariance in turbulent pipe flow

Sourabh S. Diwan[1],† **and Jonathan F. Morrison**[1]

[1]Department of Aeronautics, Imperial College London, SW7 2AZ, UK

(Received 20 October 2020; revised 20 October 2020; accepted 18 January 2021)

A three-layer asymptotic structure for turbulent pipe flow is proposed revealing, in terms of intermediate variables, the existence of a Reynolds-number-invariant logarithmic region for the streamwise mean velocity and variance. The formulation proposes a local velocity scale (which is not the friction velocity) for the intermediate layer and results in two overlap layers. We find that the near-wall overlap layer is governed by a power law for the pipe for all Reynolds numbers, whereas the log law emerges in the second overlap layer (the inertial sublayer) for sufficiently high Reynolds numbers (Re_τ). This provides a theoretical basis for explaining the presence of a power law for the mean velocity at low Re_τ and the coexistence of power and log laws at higher Re_τ. The classical von Kármán (κ) and Townsend–Perry (A_1) constants are determined from the intermediate-scaled log-law constants; κ shows a weak trend at sufficiently high Re_τ but falls within the commonly accepted uncertainty band, whereas A_1 exhibits a systematic Reynolds-number dependence until the largest available Re_τ. The key insight emerging from the analysis is that the scale separation between two adjacent layers in the pipe is proportional to $\sqrt{Re_\tau}$ (rather than Re_τ) and therefore the approach to an asymptotically invariant state can be expected to be slow.

Key words: boundary layer structure, turbulent boundary layers, pipe flow boundary layer

1. Introduction

Reynolds number similarity is an essential tool in scaling and modelling of the near-wall turbulence. One of the cornerstones in the theory of turbulent wall flows is the logarithmic ('log') variation of the mean velocity (1.1) in the inertial sublayer:

$$U^+ = \frac{1}{\kappa}\ln(y^+) + A, \tag{1.1}$$

† Present address: Department of Aerospace Engineering, Indian Institute of Science, Bangalore 560012. Email address for correspondence: sdiwan@iisc.ac.in

where $U^+ = U/u_\tau$ and $y^+ = yu_\tau/\nu$; U is the mean streamwise velocity, y is the wall-normal distance, ν is the kinematic viscosity, $u_\tau = \sqrt{\tau_w/\rho}$ is the friction velocity, τ_w is the wall shear stress and ρ is the density. In (1.1), κ is the well-known von Kármán constant and A is the additive constant. Another celebrated result in wall turbulence is Townsend's 'attached-eddy' hypothesis (Townsend 1976), which predicts a logarithmic profile for the streamwise (and spanwise) velocity variance in the inertial sublayer. For pipe flows, the log law for the streamwise variance takes the form

$$\frac{\overline{u^2}}{u_\tau^2} = B_1 - A_1 \ln\left(\frac{y}{R}\right), \tag{1.2}$$

where u is fluctuating streamwise velocity, R is the pipe radius and the overbar indicates time averaging. Here, A_1 and B_1 are constants, and A_1 is called the 'Townsend–Perry constant' (Marusic *et al.* 2013). Perry & Chong (1982) showed that the log law for the mean velocity (1.1) and that for the streamwise variance (1.2) can be derived as dual conditions using the attached-eddy formulation.

There remain some central, yet open, questions regarding the Reynolds-number invariance and universality of the von Kármán constant that have received much attention (von Kármán 1930; Townsend 1976; Nagib & Chauhan 2008; Marusic *et al.* 2010), especially for pipe flow (Wosnik, Castillo & George 2000; Bailey *et al.* 2014). Nagib & Chauhan (2008) analysed the available experimental data for pipe flow and found κ to be nearly constant, and equal to 0.41, at sufficiently high $Re_\tau (= Ru_\tau/\nu)$. Bailey *et al.* (2014) used five data sets obtained using three different measurement techniques in the Princeton Superpipe and found the best estimate for κ to be 0.4 ± 0.02. By comparison, the Reynolds-number dependence of the Townsend–Perry constant has received rather less attention; see Perry, Henbest & Chong (1986), Marusic *et al.* (2013). The theoretical analysis of Hultmark (2012), using the method of near asymptotics for $\overline{u^2}$, suggests a possible Re_τ dependence of A_1, although this is not discussed. Based on the available data, it is not clear whether there is a systematic Reynolds-number dependence of A_1 for pipe flow.

There have also been alternative formulations for the mean velocity, e.g. the power-law variation proposed by Barenblatt (1993) for pipe and channel flows. Zagarola & Smits (1998) used a general matching principle involving different velocity scales for the inner and outer layers, and argued that, as long as the ratio of the velocity scales is a function of Reynolds number, the mean velocity is expected to follow a power law. Princeton Superpipe measurements show that, at very high Reynolds numbers, $Re_\tau = O(10^5)$, a power law is present in the lower part of the overlap region followed by the log law further away from the wall; see also McKeon *et al.* (2004) and Hultmark *et al.* (2012).

Here we propose a theoretical framework, in the context of turbulent pipe flow, for addressing some of the outstanding issues outlined above. We seek Reynolds-number scaling of the mean velocity and variance in the intermediate region using the length scale, $y_m^+ \propto \sqrt{Re_\tau}$ and the velocity scale (u_m) equal to the r.m.s. velocity at $y = y_m$. We propose the existence of a distinct intermediate layer (with scales y_m and u_m), in addition to the classical inner and outer layers, implying a three-layer asymptotic structure for pipe flow. The first studies to hypothesise the presence of an intermediate or 'meso-' layer in wall turbulence, with the $\sqrt{Re_\tau}$ scaling, were due to Long & Chen (1981) and Afzal (1982). Afzal (1982) carried out asymptotic analysis for the pipe flow and identified an intermediate layer, which implied the existence of two overlap layers. Sreenivasan & Sahay (1997) argued that the mean momentum balance within the mesolayer in a pipe or channel is distinct in character from that in the classical inner and outer layers;

they employed asymptotic arguments to explore the mesolayer structure. The mean-force balance performed by Wei *et al.* (2005) shows that there exists a region, which scales on $\sqrt{Re_\tau}$, wherein the dominant balance is between the turbulent inertia, pressure gradient and viscous forces (Klewicki 2013). These studies provide a strong physical basis for the existence of the meso- or intermediate layer in pipe flow. The term mesolayer was used with a different connotation in Wosnik *et al.* (2000), namely, to provide an offset for the log-law origin in the inertial sublayer, which is not relevant to the present study. Here we use the term 'intermediate layer' as it is closer in spirit to that proposed in Afzal (1982), and define it as a layer of finite thickness centred on $y/y_m = 1$ with governing scales (y_m, u_m). We examine the consequences of intermediate variables for the scaling and structure of high-Reynolds-number pipe-flow turbulence, using the well-established principle of generalised asymptotic matching (Zagarola & Smits 1998).

2. Intermediate scaling for mean velocity and variance

The present analysis is based on the nanoscale thermal anemometry probe (NSTAP) data measured in the Princeton Superpipe (Hultmark *et al.* 2012). Figure 1 shows scaling of the streamwise variance with length scale, $y_m^+ = 3.5\sqrt{Re_\tau}$, and velocity scale, $u_m = \sqrt{\overline{u^2}}(y = y_m)$. As can be seen, there is an excellent collapse of the profiles in the region around $y/y_m = 1$ for two decades in Re_τ, $1985 \leq Re_\tau \leq 98\,190$: this is the motivation for using u_m as the intermediate velocity scale. At the highest Reynolds numbers, the scaled region extends from $0.15 \leq y/y_m \leq 15$ and, as expected, the profiles peel off from this trend on both sides of $y/y_m = 1$ as Re_τ decreases. The choice of constant used in the definition of y_m^+ is guided by the coefficients for $\sqrt{Re_\tau}$ used in previous definitions of the mesolayer location, e.g. $2\sqrt{Re_\tau}$ (Sreenivasan & Sahay 1997), or in determining the lower bound of the inertial sublayer, $3\sqrt{Re_\tau}$ (Marusic *et al.* 2013). Here, a slightly higher value, 3.5, is chosen to provide a better Re_τ scaling of the variance profiles for the pipe as well as boundary layer data (not shown); see Diwan & Morrison (2019). Note that the qualitative (and, to certain extent, quantitative) nature of the results is unaffected by the precise choice of this constant. Taking U_m as the mean velocity at $y = y_m$, figure 2 shows, in 'defect' form, the corresponding mean velocity profiles scaled on u_m. Excellent scaling is apparent around $y/y_m = 1$ for mean velocity also. This scaling for the mean velocity and variance suggests the existence of a distinct, asymptotic intermediate layer lying between the classical inner and outer layers. This implies that there exists two overlap regions: one between the inner and intermediate layers ('Overlap Layer I') and the other between the intermediate and outer layers ('Overlap Layer II'); see also Afzal (1982). We choose the velocity scales in the inner and outer layers as u_i and u_o, respectively, which in general need not be the same as u_m. This is in contrast to the earlier formulations (Afzal 1982; Sreenivasan & Sahay 1997; Klewicki 2013), which used the same velocity scale, u_τ, for all the layers considered. The use of u_m instead of u_τ in our formulation enables the demonstration of Reynolds-number similarity in the intermediate layer of the pipe (figures 1, 2). Note that the five-layer description based on spectral characteristics of the streamwise velocity proposed by Vallikivi, Ganapathisubramani & Smits (2015) is different in spirit to the present formulation which, including the two overlap layers, also proposes a total of five layers. Next, we carry out a matching analysis using the method used by Zagarola & Smits (1998). For Overlap Layer I, the inner and intermediate scaling laws are written as

$$U^+ = f(y^+), \quad \frac{U - U_m}{u_m} = g(\zeta), \tag{2.1a,b}$$

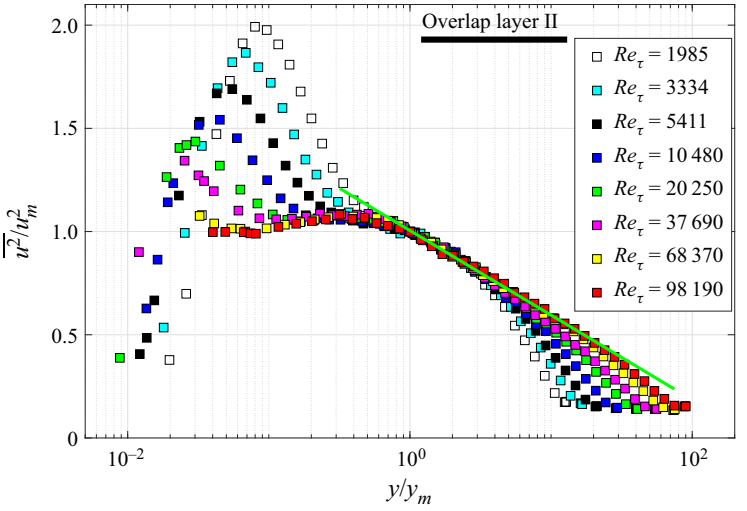

Figure 1. Streamwise variance profiles in a smooth pipe scaled on the intermediate variables y_m and u_m; data from Hultmark *et al.* (2012). The solid line is the log-law fit.

where $\zeta = y/y_m$. Asymptotic matching of the velocity gradient for the inner and intermediate layers gives

$$y^+ f'(y^+) = \Lambda_I \zeta g'(\zeta), \tag{2.2}$$

where $\Lambda_I = u_m/u_\tau$ and $(')$ indicates the derivative with respect to the corresponding independent variable. When Λ_I is Reynolds-number dependent, (2.2) does not imply log-law scaling. For this case, Reynolds-number similarity can be achieved by simultaneously matching both velocity and velocity gradient in the overlap region. This results in a power law for the mean velocity:

$$\left.\begin{aligned} f(y^+) = U^+ &= C(y^+)^\gamma, \\ \frac{U_m}{u_m} + g(\zeta) = \frac{U}{u_m} &= C_m \left(\frac{y}{y_m}\right)^\gamma, \end{aligned}\right\} \tag{2.3}$$

where γ, C and C_m are constants. Alternatively, when Λ_I = constant, a log law is obtained in the overlap region.

Figure 3(*a*) shows the variation of Λ_I with Reynolds number, where it continues to increase even at the highest Re_τ. This implies that Overlap Layer I is governed by a power law up to $Re_\tau \approx 10^5$. The ratio U_m/u_m shows a much weaker variation with Re_τ than Λ_I, without a monotonic trend (figure 3*b*): there is only a 6 % variation in U_m/u_m for two decades of change in Re_τ; this justifies the power law in (2.3). Fitting a power-law curve to U/u_m for $0.06 \leq y/y_m \leq 0.8$, $Re_\tau = 98\,190$ gives the power-law constants as $\gamma = 0.14$ and $C_m = 8.51$. Note that γ is independent of Re_τ, whereas C_m shows a weak Re_τ-dependence reflecting the weak trend of U_m/u_m with Re_τ (figure 3*b*). Using these parameters, the variation of $(U - U_m)/u_m$ is plotted in figure 2 as a magenta line which fits the data quite well in Overlap Layer I. To determine C, we separately fit a power law to the inner-scaled data (not shown here) for $Re_\tau = 98\,190$ in the corresponding range, $65 \leq y^+ \leq 880$ (Hultmark *et al.* 2012). This yields the same value of $\gamma = 0.14$, with $C = 8.47$. These are close to the values $\gamma = 0.142$ and $C = 8.48$ reported by McKeon *et al.* (2004). Overlap Layer II is bounded by the intermediate layer and the outer layer.

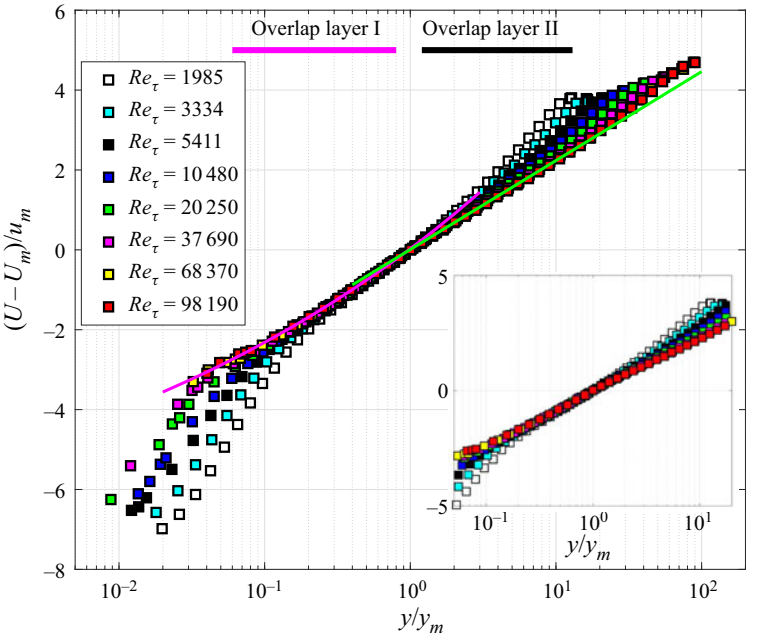

Figure 2. Streamwise mean velocity deficit scaled on the intermediate variables. The magenta line indicates a power-law fit and the green line indicates the log-law fit. The inset shows the variation without the power and log law lines.

The scaling law for the mean velocity deficit in the outer layer can be written as

$$\frac{U_{CL} - U}{u_o} = h\left(\frac{y}{R}\right), \tag{2.4}$$

where U_{CL} is the pipe centre-line velocity. It can be seen that the character of the mean velocity variation in Overlap Layer II is determined by the velocity-scale ratio, $\Lambda_{II} = u_o/u_m$ (corresponding to Λ_I in 2.2). Note that although (2.4) is written in a Reynolds-number-invariant form, the appropriate velocity scale, u_o, that would result in Reynolds-number similarity in the outer region is still unknown (Morrison *et al.* 2004). The two alternatives for u_o that have been used so far, for the pipe, are u_τ and $U_{CL} - U_b$ (Zagarola & Smits 1998), where U_b is the bulk velocity. Choosing $u_o = u_\tau$, $\Lambda_{II} = 1/\Lambda_I$, implying (figure 3*a*) that Overlap Layer II is also governed by a power law for the entire Re_τ range. This would be a surprising result as there has been overwhelming support in favour of the log law. If, on the other hand, we choose $u_o = (U_{CL} - U_b)$, we get $\Lambda_{II} = (U_{CL} - U_b)/u_m$, see figure 3(*c*), which shows that Λ_{II} is a strong function of Re_τ, but where, for $Re_\tau \gtrsim 10^4$, it shows a much weaker dependence on Re_τ. If we assume Λ_{II} to be approximately constant for $Re_\tau \gtrsim 10^4$, we recover the log law for the mean velocity in Overlap Layer II, which, in terms of u_m and y_m, can be written as

$$\frac{U - U_m}{u_m} = \frac{1}{\kappa_m} \ln\left(\frac{y}{y_m}\right) + A_m. \tag{2.5}$$

To obtain κ_m and A_m, we fit a least-square straight line through the mean velocity data (green solid line in figure 2) for the two highest Reynolds numbers, $Re_\tau = 68\,370$ and $Re_\tau = 98\,190$, and for $1.2 \leq (y/y_m) \leq 13$, equivalent to $4.2\sqrt{Re_\tau} \leq y^+ \leq 0.145Re_\tau$ for

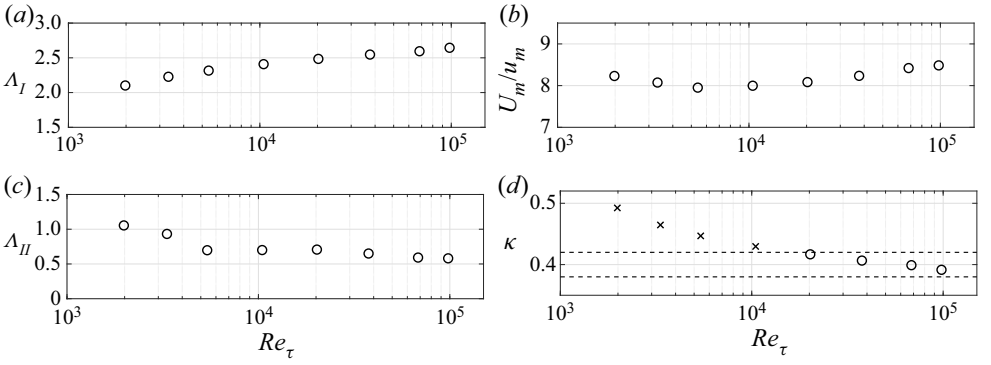

Figure 3. Variation with Re_τ of (*a*) $\Lambda_I = u_m/u_\tau$, (*b*) U_m/u_m, (*c*) $\Lambda_{II} = (U_{CL} - U_b)/u_m$, (*d*) κ obtained from (3.1*a*,*b*); the values of κ for $Re_\tau \lesssim 10^4$ do not correspond to the log law and are shown by crosses.

$Re_\tau = 98\,190$, which is broadly consistent with the range used in Marusic *et al.* (2013). The fit gives the following values for the constants:

$$\kappa_m = 1.034, \quad A_m = 0.0084. \tag{2.6a,b}$$

These represent the Reynolds-number-invariant log-law constants in terms of the intermediate variables for $Re_\tau \gtrsim 10^4$. Note that, provided the Reynolds-number similarity in the intermediate layer is ensured, the value of κ_m is independent of small changes in the numerical value of the coefficient in the definition of y_m. The value of A_m, however, is directly dependent on this choice (2.5). Moreover, the range $1.2 \leq (y/y_m) \leq 13$ is valid only for the two highest Re_τ. As Re_τ decreases, the range of y/y_m over which a log variation is observed continues to decrease, although κ_m and A_m remain the same, as clearly seen in figure 2. To further support this observation, we plot the variation of an 'indicator function' (McKeon *et al.* 2004) with Re_τ, which is presented as supplementary material to this paper available at https://doi.org/10.1017/jfm.2021.71.

In figure 1, the Reynolds-number similarity of the streamwise variance for $y \approx y_m$ implies that, for $y > y_m$, there should exist a Reynolds-number-invariant log law for the variance as well (scaled on the intermediate variables), which is

$$\frac{\overline{u^2}}{u_m^2} = B_1^m - A_1^m \ln\left(\frac{y}{y_m}\right). \tag{2.7}$$

To determine A_1^m and B_1^m, we fit a least-square straight line through the points in figure 1 (shown as a solid line) in the region $1.2 \leq y/y_m \leq 13$ for the two highest Reynolds numbers; this range is the same as that chosen for fitting the log law for the mean velocity in Overlap Layer II (figure 2). Again the extent of the log region for the variance decreases with decrease in Re_τ; see the supplementary material for the indicator-function plots. (The behaviour of $\overline{u^2}$ in Overlap Layer I is beyond the scope of the present work.) This line fit gives the Re-invariant log-law constants for the streamwise variance as

$$A_1^m = 0.178, \quad B_1^m = 1.005. \tag{2.8a,b}$$

We do not attempt to estimate the uncertainty bounds for A_1^m and B_1^m, nor for κ_m and A_m, (2.6*a*,*b*) here, as their precise numerical values are not relevant for our key conclusions.

Re_τ	κ	A	A_1	B_1
1985	×	×	0.79	2.44
3334	×	×	0.88	2.51
5411	×	×	0.95	2.48
10 480	×	×	1.03	2.34
20 250	0.42	5.17	1.1	2.13
37 690	0.41	4.92	1.15	1.88
68 370	0.4	4.75	1.2	1.59
98 190	0.39	4.55	1.24	1.43

Table 1. The log-law constants for the mean velocity (κ and A) and variance (A_1 and B_1) obtained from (3.1*a*,*b*) and (3.2*a*,*b*) using the log fits in (2.5) and (2.7). For $Re_\tau \leq 10,480$, κ and A are shown as '×' as log law is not expected in Overlap Layer II (figure 3*d*).

3. Consequences for the von Kármán and Townsend–Perry 'constants'

The classical log-law constants for the mean velocity and variance can be readily expressed in terms of the constants obtained from the intermediate-scaled log laws. For the mean velocity, this relation can be written as (1.1), (2.5)

$$\kappa = \frac{\kappa_m}{(u_m/u_\tau)}, \quad A = \frac{u_m}{u_\tau}\left\{\left[\frac{U_m}{u_m} + A_m\right] - \frac{1}{\kappa_m}\ln(y_m^+)\right\}. \tag{3.1a,b}$$

The value of κ obtained from (3.1*a*,*b*) is plotted in figure 3(*d*); see also table 1. For $Re_\tau > 2 \times 10^4$, κ falls within the range 0.4 ± 0.02 (Bailey *et al.* 2014), shown as dashed lines in the figure; the trend exhibited by κ within the band reflects the variation of u_m/u_τ with Re_τ (figure 3*a*; 3.1*a*,*b*). For $Re_\tau < 10^4$, the values of κ are found to be much higher than those which could be reasonably associated with a log law. These are denoted as crosses in figure 3(*d*), including $\kappa = 0.43$ at $Re_\tau = 10\,480$ which falls beyond the band of 0.4 ± 0.02. This suggests that the mean velocity profile in Overlap Layer II is better described by a power law at lower Re_τ, as implied by the strong Reynolds-number dependence of Λ_{II} for $Re_\tau \lesssim 10^4$ (figure 3*c*). Note that Overlap Layer I is governed by power law for all Re_τ considered here. For $Re_\tau < 10^4$, the two overlap layers may not be entirely distinct and therefore the two power-law profiles may appear indistinguishable (figure 2). These results are consistent with those in Zagarola & Smits (1998) and McKeon *et al.* (2004).

The presence of a power law in Overlap Layer I and of the log law in Overlap Layer II, for $Re_\tau > 2 \times 10^4$, supports the observation by Zagarola & Smits (1998) (see also Hultmark *et al.* 2012) that, at high Re_τ, the mean velocity initially follows a power law, with a log law at larger y. Note that in their analysis, the power and log laws share the same overlap region, whereas in the present three-layer formulation they occupy two different overlap regions. This provides an explanation for the coexistence of the power and log-law profiles in the pipe flow at a given (and sufficiently large) Re_τ. Furthermore, since the length scale for the intermediate layer is $\propto \sqrt{Re_\tau}$, the lower limit for the log law for the mean velocity should be Reynolds-number dependent, rather than constant in wall variables: see the discussion in Marusic *et al.* (2013) and Bailey *et al.* (2014).

For the variance, the classical constants, A_1 and B_1 (1.2), can be expressed in terms of A_1^m and B_1^m (2.7) as

$$A_1 = A_1^m\left(\frac{u_m^2}{u_\tau^2}\right), \quad B_1 = \left[A_1^m \ln\left(\frac{y_m}{R}\right) + B_1^m\right]\left(\frac{u_m^2}{u_\tau^2}\right). \tag{3.2a,b}$$

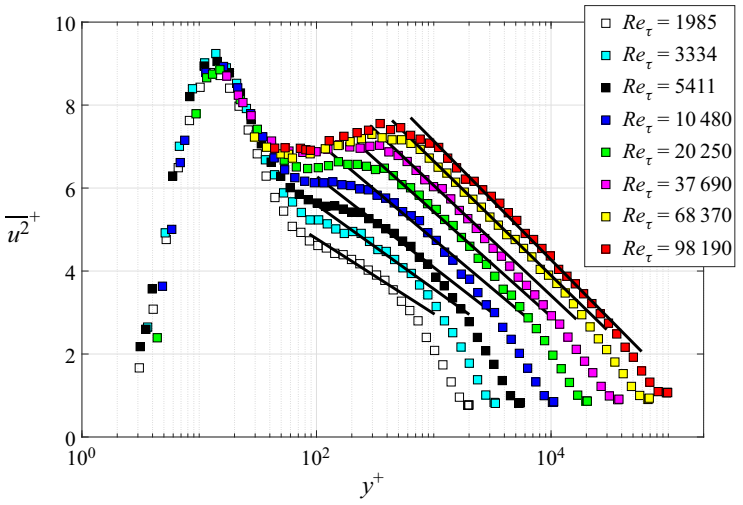

Figure 4. Streamwise variance profiles for the pipe; solid lines are the classical log-law fits using A_1 and B_1 from table 1.

Values of A_1 and B_1 calculated from (3.2*a*,*b*) (with $A_1^m = 0.178$ and $B_1^m = 1.005$) are included in table 1; a clear trend in A_1 and B_1 with respect to Re_τ is evident. Figure 4 shows the log-law fits to the variance, in wall variables, obtained by using A_1 and B_1 from table 1. As can be seen, the log fits inferred from (3.2*a*,*b*) show a good match with the measured profiles in the intermediate region, over the entire Re_τ range. This leads us to conclude that the Townsend–Perry 'constant', A_1, actually shows a systematic dependence on Re_τ even for $Re_\tau > 10^4$. This is due to the fact that A_1^m and B_1^m are Re_τ-invariant and that u_m/u_τ (figure 3*a*) and y_m/R $(= 3.5/\sqrt{Re_\tau})$ show a continuous dependence on Re_τ. Furthermore, the values of A_1 in table 1 are entirely consistent, at corresponding Reynolds numbers, with those in Perry *et al.* (1986) ($A_1 = 0.9$ for $Re_\tau \leq 3900$) and Hultmark *et al.* (2012) ($A_1 = 1.25$ for $Re_\tau = 98\,190$; Marusic *et al.* (2013) reported $A_1 = 1.23 \pm 0.05$ for the same Re_τ). Hence, the use of the three-layer formulation and intermediate scaling enable us to explain the Re_τ-dependence of A_1, providing both an explanation for the low values of A_1 obtained by Perry *et al.* (1986), as well as reproducing $A_1 \approx 1.25$ for the high-Re data. Another advantage of this framework is that the extent of the log region for different Re_τ in the classical scaling (figure 4) is automatically determined once the extent of the intermediate-scaled log law (2.7), (3.2*a*,*b*) is known. This removes the subjectivity of fitting a log law to the variance data, which has a direct bearing on the determination of A_1. The same considerations also apply to the determination of κ for the mean velocity (table 1).

Note that the values of A_1 and B_1 are listed for all Re_τ in table 1, whereas those for κ and A are listed only for $Re_\tau > 2 \times 10^4$, below which we expect a power law. However, there is no general principle to rule out the presence of log law in $\overline{u^2}$ at $Re_\tau \lesssim 10^4$ apart from low-Reynolds-number effects. In addition, indicator functions for $\overline{u^2}$ suggest the presence of a log law for the entire range of Re_τ. Of course, the numerical values of κ and A_1 (and also A and B_1) in table 1 and their precise variation with Re_τ are contingent on the accuracy of the data used for fitting the intermediate-scaled log laws. Vallikivi (2014) estimates uncertainties in the NSTAP measurement, U, to be $\pm 2.2\,\%$, the corresponding uncertainty in $\overline{u^2}$ being $\pm 3.0\,\%$. Using the mean momentum equation, the associated error in $\overline{uv}$

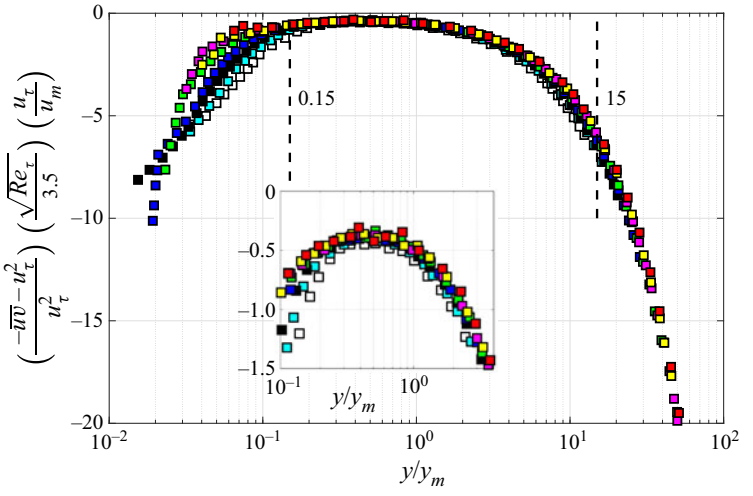

Figure 5. The deficit in $-\overline{uv}$ scaled on the intermediate variables, i.e. $3.5/\sqrt{Re_\tau}(= y_m/R)$ and u_m/u_τ, as a function of y/y_m. See figure 4 for the legend.

(where v is the radial velocity component) is expected to be approximately $\pm 5\,\%$. These estimates can be usefully compared to the Pitot probe data from McKeon (2004) which estimates the corresponding uncertainties in U to be $\pm 0.3\,\%$. However, here obviously one does not have the higher-order statistics provided by the NSTAP probe. Nonetheless, as table 1 shows, the present analysis using the NSTAP data provides estimates of κ and A that are consistent with the earlier Pitot probe data from the Superpipe. We therefore expect the three-layer structure to be apparent for both data sets.

4. Discussion

The choice of u_m as a velocity scale is not obvious, the u-component comprising both the 'active' shear-stress-bearing motion of the inner layer (the 'large-scale motions', LSM) and that induced by the 'very-large-scale motions' (VLSM) residing primarily in the outer layer (Marusic *et al.* 2010). The intermediate layer can be conceived as a region in which both the LSM and VLSM are of comparable magnitude, as suggested by the spectral analysis of Vallikivi *et al.* (2015). Thus, the intermediate layer in pipe flow is a central site for inner-outer interaction (Morrison 2007; Marusic *et al.* 2010). Further, the peak in shear stress, $-\overline{uv}$ (figure 5), is close to the outer peak in $\overline{u^2}$ (figure 1), which is the lower limit to the log law; see figure 6. The log region makes a major contribution to the bulk production of turbulence kinetic energy at high Re_τ, and is likely to enhance levels of $\overline{u^2}$ in the intermediate region (Hultmark *et al.* 2012). The causal connection between $-\overline{uv}$ and $\overline{u^2}$ in a fully developed internal flow is clearly provided through the production of $\overline{u^2}$, $\overline{uv}(\mathrm{d}U/\mathrm{d}y)$. More specifically, we note that, in the local-equilibrium region, the non-dimensional dissipation rate, $\epsilon/u_\tau^3/R \propto \sqrt{Re_\tau}$ (Morrison & Fernandez Vicente 2019), implying that u_m, as a scale for $\overline{u^2}$, is also relevant to $-\overline{uv}$.

We consider the mean momentum balance for the turbulent pipe flow as follows:

$$\nu\frac{\mathrm{d}^2U}{\mathrm{d}y^2}+\frac{\mathrm{d}}{\mathrm{d}y}(-\overline{uv})=-\frac{u_\tau^2}{R}\left(\equiv\frac{1}{\rho}\frac{\mathrm{d}p}{\mathrm{d}x}\right). \tag{4.1}$$

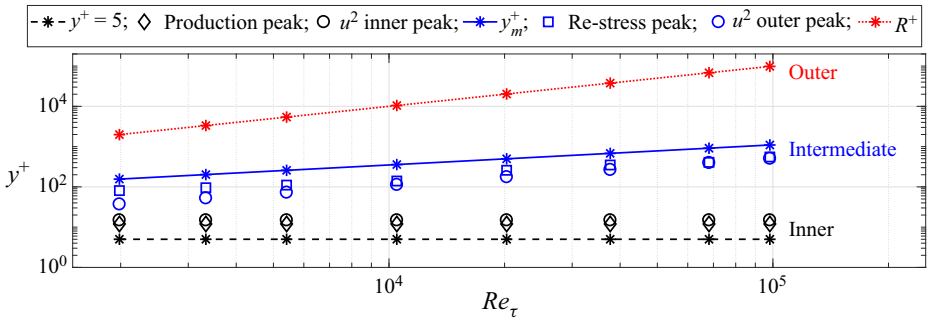

Figure 6. Variation of three length scales, $y^+ = 5$, y_m^+, R^+, and locations of peaks in $-\overline{uv}$, $-\overline{uv}(\mathrm{d}U/\mathrm{d}y)$ and $\overline{u^2}$. There is some uncertainty in determining the location of the peak in $-\overline{uv}$ for the two largest Re_τ (figure 5 inset), which is typically the same as the size of the symbols.

Its scaling behaviour in the classical inner and outer layers is well-known (Afzal 1982; Klewicki 2013). To investigate the leading-order force balance in the intermediate layer, we introduce the intermediate-scaled mean velocity deficit (2.1*a*,*b*). For scaling the Reynolds stress gradient, we use the observation that the deficit in the maximum Reynolds shear stress, $(-\overline{uv}_{max} - u_\tau^2)/u_\tau^2$, scales on $1/\sqrt{Re_\tau}$ (Afzal 1982; Sreenivasan & Sahay 1997). With intermediate scaling, (4.1) can be rearranged in deficit form as:

$$\frac{1}{(3.5)^2}\frac{\mathrm{d}^2}{\mathrm{d}\zeta^2}\left(\frac{U-U_m}{u_m}\right) + \frac{\mathrm{d}}{\mathrm{d}\zeta}\left[\left(\frac{-\overline{uv}-u_\tau^2}{u_\tau^2}\right)\left(\frac{\sqrt{Re_\tau}}{3.5}\right)\frac{u_\tau}{u_m}\right] = -\frac{u_\tau}{u_m}. \tag{4.2}$$

The quantity in square brackets on the left-hand side in (4.2), the Reynolds-stress deficit, is plotted in figure 5 as a function of $\zeta = y/y_m$; the inset shows an expanded view of the peak in $-\overline{uv}$. The $-\overline{uv}$ data are obtained from (4.1) using the mean velocity data (figure 2): figure 5 shows that intermediate scales work well in the intermediate layer. This collapse is consistent with that seen earlier for $\overline{u^2}$ (figure 1) and $(U - U_m)$ (figure 2). The term u_τ/u_m on the right-hand side of (4.2) implies that the leading-order force balance, under the intermediate scaling, is approximate so long as u_τ/u_m is a function of Re_τ, and can be expected to become exact as $Re_\tau \to \infty$. However, it is clear that the intermediate scaling presents a 'distinguished limit' distinct from the inner and outer limits (Afzal 1982). If the ratio $\Lambda_I = u_m/u_\tau$ (and $\Lambda_{II} = u_o/u_m$) reaches a constant value as $Re_\tau \to \infty$, the present analysis becomes identical with that in Afzal (1982), with all the three layers governed by u_τ. Clearly this limit has not yet been reached for the present data, as u_m continues to be a relevant velocity scale in the intermediate layer even for $Re_\tau = O(10^5)$; see figures 1–3. Note that the balance of forces in (4.2) is consistent with that obtained in layer III in the analysis of Klewicki (2013).

As a distinguished limit, the intermediate layer has distinct underlying physics, unique to its position in the wall layer. This becomes evident by looking at figure 6, which plots positions of the three layers in relation to locations of peaks in $-\overline{uv}$, $-\overline{uv}(\mathrm{d}U/\mathrm{d}y)$ and $\overline{u^2}$. As can be seen, the peak in production ($y^+ = 12$) and the inner peak in $\overline{u^2}$ ($y^+ \approx 15$; Hultmark *et al.* 2012) characterise the inner layer. Correspondingly, the peak in Reynolds shear stress and the outer peak in $\overline{u^2}$ (given by $y^+ = 0.23(Re_\tau)^{0.67}$; Hultmark *et al.* 2012) are seen to characterise the intermediate layer; see figure 6. The intermediate layer is amenable to another interesting physical interpretation: in the context of their mesolayer theory, Sreenivasan & Sahay (1997) proposed that the peak in $-\overline{uv}$ could play a role similar to that of the 'critical layer' in unstable wall flows. They pointed out that the

mean velocity at the $(-\overline{uv})_{max}$ location is approximately a constant fraction ($= 0.65$) of the centre-line velocity in the pipe, similar to that for a critical layer. In the present work, U_m/U_{CL} falls in the range 0.68–0.64 for $Re_\tau = 1985$–$98\,190$ and for $Re_\tau > 20\,000$, $U_m/U_{CL} \approx 0.65$.

5. Conclusion

We have shown that, using intermediate variables (y_m, u_m), the streamwise mean velocity deficit and variance exhibit Reynolds-number similarity in the intermediate region of the pipe flow. This suggests a three-layer asymptotic formulation for pipe flow, with two overlap layers (Afzal 1982), wherein the intermediate layer is governed by a velocity scale (u_m) different from the friction velocity. A generalised matching analysis shows that Overlap Layer I (nearer to the wall) is governed by a power law for the mean velocity until $Re_\tau = O(10^5)$ and that the log law emerges in Overlap Layer II for $Re_\tau \gtrsim 10^4$. This provides a theoretical explanation for the presence of a power law close to the wall and a log law further away, as observed in the Superpipe measurements of Zagarola & Smits (1998) and Hultmark *et al.* (2012).

In terms of the intermediate scaling, Overlap Layer II (which represents the inertial sublayer) exhibits a Reynolds-number-invariant log law for the mean velocity deficit (at high Re_τ) as well as the variance. The von Kármán (κ) and Townsend–Perry (A_1) 'constants' have been derived from the intermediate-scaled log-law constants. We find that κ shows a weak trend within the range 0.4 ± 0.02 for $Re_\tau > 2 \times 10^4$ consistent with the literature, whereas A_1 exhibits a systematic Reynolds-number dependence up to the highest available Re_τ. The present formulation shows that the scale separation between two adjacent layers is proportional to $\sqrt{Re_\tau}$ (rather than Re_τ) and this is likely to explain the slow approach to asymptotic conditions (in terms of classical variables) evident in the pipe flow data.

Supplementary material. Supplementary material is available at https://doi.org/10.1017/jfm.2021.71.

Acknowledgements. We are grateful to Professor A. Smits for use of the NSTAP data and for useful discussions. We thank Professor J. Klewicki for his comments on the mean momentum analysis, and the referees for useful suggestions that have helped to improve the paper.

Funding. We acknowledge financial support from EPSRC under Grant No. EP/I037938/1.

Declaration of interests. The authors report no conflict of interest.

Author ORCIDs.
Sourabh S. Diwan https://orcid.org/0000-0002-9190-7403;
Jonathan F. Morrison https://orcid.org/0000-0003-3688-9860.

References

Afzal, N. 1982 Fully developed turbulent flow in a pipe: an intermediate layer. *Ing.-Arch.* **52**, 355–377.

Bailey, S.C.C., Vallikivi, M., Hultmark, M. & Smits, A.J. 2014 Estimating the value of von Kármán's constant in turbulent pipe flow. *J. Fluid Mech.* **749**, 79–98.

Barenblatt, G.I. 1993 Scaling laws for fully developed shear flows. Part 1. Basic hypotheses and analysis. *J. Fluid Mech.* **248**, 513–520.

Diwan, S.S. & Morrison, J.F. 2019 Reynolds-number dependence of the Townsend-Perry 'constant' in wall turbulence. In *11th International Symposium on Turbulence and Shear Flow Phenomena*. Begel House.

Hultmark, M. 2012 A theory for the streamwise turbulent fluctuations in high Reynolds number pipe flow. *J. Fluid Mech.* **707**, 575–584.

Hultmark, M., Vallikivi, M., Bailey, S.C.C. & Smits, A.J. 2012 Turbulent pipe flow at extreme Reynolds numbers. *Phys. Rev. Lett.* **108**, 094501.

VON KÁRMÁN, T. 1930 Mechanische Ahnlichkeit und Turbulenz. *Gott. Nachr.* **1**, 58–76.
KLEWICKI, J.C. 2013 Self-similar mean dynamics in turbulent wall flows. *J. Fluid Mech.* **718**, 596–621.
LONG, R.R. & CHEN, T.-C. 1981 Experimental evidence for the existence of the 'mesolayer' in turbulent systems. *J. Fluid Mech.* **105**, 19–59.
MARUSIC, I., MCKEON, B.J., MONKEWITZ, P.A., NAGIB, H.M., SMITS, A.J. & SREENIVASAN, K.R. 2010 Wall-bounded turbulent flows at high Reynolds numbers: recent advances and key issues. *Phy. Fluids* **22**, 065103.
MARUSIC, I., MONTY, J.P., HULTMARK, M. & SMITS, A.J. 2013 On the logarithmic region in wall turbulence. *J. Fluid Mech.* **716**, R3.
MCKEON, B.J. 2004 High Reynolds number turbulent pipe flow. PhD thesis, Princeton University.
MCKEON, B.J., LI, J., JIANG, W., MORRISON, J.F. & SMITS, A.J. 2004 Further observations on the mean velocity distribution in fully developed pipe flow. *J. Fluid Mech.* **501**, 135–147.
MORRISON, J.F. 2007 The interaction between inner and outer regions of wall-bounded flow. *Phil. Trans. R Soc. Lond.* A **365**, 683–698.
MORRISON, J.F. & FERNANDEZ VICENTE, J. 2019 The energy budget at the outer peak of $\overline{u^2}$ in turbulent pipe flow. In *APS DFD G11.00006*. American Physical Society.
MORRISON, J.F., MCKEON, B.J., JIANG, W. & SMITS, A.J. 2004 Scaling of the streamwise velocity component in turbulent pipe flow. *J. Fluid Mech.* **508**, 99–131.
NAGIB, H.M. & CHAUHAN, K.A. 2008 Variations of von Kármán coefficient in canonical flows. *Phy. Fluids* **20**, 101518.
PERRY, A.E. & CHONG, M.S. 1982 On the mechanism of wall turbulence. *J. Fluid Mech.* **119**, 173–217.
PERRY, A.E., HENBEST, S. & CHONG, M.S. 1986 A theoretical and experimental study of wall turbulence. *J. Fluid Mech.* **165**, 163–199.
SREENIVASAN, K.R. & SAHAY, A. 1997 The persistence of viscous effects in the overlap region, and the mean velocity in turbulent pipe and channel flows. In *Self-Sustaining Mechanisms of Wall Turbulence* (ed. R. Panton), pp. 253–272. Computational Mechanics Publications.
TOWNSEND, A.A. 1976 *The Structure of Turbulent Shear Flow*. Cambridge University Press.
VALLIKIVI, M. 2014 Wall-bounded turbulence at high Reynolds numbers. PhD thesis, Princeton University.
VALLIKIVI, M., GANAPATHISUBRAMANI, B. & SMITS, A.J. 2015 Spectral scaling in boundary layers and pipes at very high Reynolds numbers. *J. Fluid Mech.* **771**, 303–326.
WEI, T., FIFE, P., KLEWICKI, J. & MCMURTRY, P. 2005 Properties of the mean momentum balance in turbulent boundary layer, pipe and channel flows. *J. Fluid Mech.* **522**, 303–327.
WOSNIK, M., CASTILLO, L. & GEORGE, W.K. 2000 A theory for turbulent pipe and channel flows. *J. Fluid Mech.* **421**, 115–145.
ZAGAROLA, M.V. & SMITS, A.J. 1998 Mean-flow scaling of turbulent pipe flow. *J. Fluid Mech.* **373**, 33–79.